ORIGINAL ARTICLE

Assessment of troposphere mapping functions using three-dimensional ray-tracing

Landon Urquhart · Felipe G. Nievinski ·
Marcelo C. Santos

Abstract The troposphere delay is an important source of error for precise GNSS positioning due to its high correlation with the station height parameter. It has been demonstrated that errors in mapping functions can cause sub-annual biases as well as affect the repeatability of GNSS solutions, which is a particular concern for geophysical studies. Three-dimensional ray-tracing through numerical weather models (NWM) is an excellent approach for capturing the directional and daily variation of the tropospheric delay. Due to computational complexity, its use for positioning purposes is limited, but it is an excellent tool for evaluating current state-of-the-art mapping functions used for geodetic positioning. Many mapping functions have been recommended in the past such as the Niell Mapping Function (NMF), Vienna Mapping Function 1 (VMF1), and the Global Mapping Function (GMF), which have been adopted by most IGS analysis centers. A new Global Pressure Temperature model (GPT2) has also been developed, which has been shown to improve upon the original atmospheric model used for the GMF. Although the mapping functions mentioned above use the same functional formulation, they vary in terms of their atmospheric source and calibration approach. A homogeneous data set of three-dimensional ray-traced delays is used to evaluate all components of the mapping functions, including their underlying functional formulation, calibration, and compression method. Additionally, an alternative representation of the VMF1 is generated using the same atmospheric source as the truth data set to evaluate the differences in ray-tracing methods and their effect on the end mapping function. The results of this investigation continue to support the use of the VMF1 as the mapping function of choice when geodetic parameters are of interest. Further support for the GPT2 and GMF as reliable back-ups when the VMF1 is not available was found due to their high consistency with the NWM-derived mapping function. Additionally, a small latitude-dependent bias in station height was found in the current mapping functions. This bias was identified to be due to the assumption of a constant radius of the earth and was largest at the poles and at the equator. Finally, an alternative version of the VMF1 is introduced, namely the UNB-VMF1 which provides users with an independent NWM-derived mapping function to support geodetic positioning.

Keywords Troposphere · Numerical weather models · Mapping functions

L. Urquhart · M. C. Santos
Department of Geodesy and Geomatics Engineering,
University of New Brunswick, Fredericton, Canada

Present Address:
L. Urquhart (✉)
Nexteq Navigation, Calgary, Canada
e-mail: lurquhart@nexteqnav.com

F. G. Nievinski
Department of Aerospace Engineering Sciences,
University of Colorado, Boulder, CO, USA

Introduction

The tropospheric delay is an important error source for precise geodetic positioning as it affects both the accuracy and repeatability of station coordinates as well as causing differences in the annual periodic signals of geodetic time series (Tesmer et al. 2007; Vey et al. 2006). As the troposphere is a non-dispersive medium for Global Navigation Satellite System (GNSS) frequencies, it cannot be removed by observing on multiple frequencies, thus it is necessary to model the delay using external parameters.

For modeling purposes, the delay can be decomposed into a zenith component and slant factor, often referred to as a mapping function, which maps the zenith delay from the vertical to the elevation angle of the observations. For positioning purposes, both zenith delay modeling and mapping functions have an important role. In this contribution, we set aside the modeling of zenith delays and focus our efforts on modeling the elevation angle dependence of the neutral atmosphere via mapping functions. The most commonly used mapping functions today include the Niell Mapping Function (NMF) (Niell 1996), the Global Mapping Functions (GMF) (Boehm et al. 2006a), the Vienna Mapping Functions 1 (VMF1) (Boehm et al. 2006b), and most recently the GPT2 empirical slant delay model (Lagler et al. 2013).

Three-dimensional ray-tracing through numerical weather models (NWM) can provide a realistic representation of the slant delay on sub-daily basis, including both the elevation angle and azimuth dependence of the troposphere delay (Urquhart et al. 2012). Due to the large computational burden, the application of direct ray-tracing for positioning purposes is fairly restricted, but ray-tracing can act as a rigorous benchmark for evaluating mapping functions. For this reason, a three-dimensional ray-tracing campaign was undertaken to assess both the realization and underlying functional formulation of the current state-of-the-art mapping functions.

Our objective is to assess the functional formulation, atmospheric models, ray-tracing algorithms, and slant factor compression methods underlying the current state-of-the-art mapping. In addition, a new realization of the VMF1, referred to as the UNB-VMF1, is introduced and evaluated, which will help assess the impact of differences in the atmospheric model and the ray-tracing algorithms on the derived mapping functions.

We begin by describing the tropospheric delay and the modeling of mapping functions for geodetic purposes. Section "Experiment description" provides a description of the ray-tracing campaign used to evaluate the functional formulations and mapping functions. Finally, Section "Results and discussion" presents the results and discussion.

The tropospheric delay

The total tropospheric delay (ΔL) is defined as the difference between the apparent ray-path length and the geometric distance:

$$\Delta L = \int_{\substack{\text{bent} \\ \text{raypath}}} n(\ell)\mathrm{d}\ell - \int_{\substack{\text{straight} \\ \text{line}}} 1\mathrm{d}\ell \tag{1}$$

where the bent ray-path is the actual path of the ray, from the satellite propagating through the atmosphere down to the receiver, and the straight line corresponds to the idealized ray-path in a vacuum. The refractive index, n, of a packet of moist air, more conveniently written as the refractivity (N), is given as:

$$N = 10^6(n-1) = \frac{K_1 P_\mathrm{d}}{T} + \frac{K_2 P_\mathrm{w}}{T} + \frac{K_3 P_\mathrm{w}}{T^2} \tag{2}$$

where P_d and P_w are the partial pressures due to dry gases and water vapor (in pascals), T is temperature (in kelvin), and K_1, K, and K_3 are empirically determined coefficients as given by Rüeger (2002).

Most often, the total slant delay is decomposed as:

$$\Delta L = \Delta L_\mathrm{h}^z \cdot k_\mathrm{h} + \Delta L_\mathrm{nh}^z \cdot k_\mathrm{nh} \tag{3}$$

where ΔL^z is the zenith total delay and k is the slant factor. The zenith delay and slant factor can be separated into a hydrostatic and non-hydrostatic component represented by the subscript "h" and "nh," respectively. The geometric delay, which cannot be separated into a hydrostatic and non-hydrostatic component, is grouped with the hydrostatic component in (3). The hydrostatic zenith delay component can be predicted accurately using in situ measurements or from a NWM. On the other hand, non-hydrostatic zenith delay component is more difficult to model accurately and is therefore estimated as an unknown along with other geodetic quantities of interest.

The slant factor accounts for the elevation angle and possibly azimuthal dependence of the slant delay. A mapping function can be considered a slant factor model; in other words, a slant factor value can be obtained by evaluating a mapping function for specific input conditions.

Underlying all mapping functions is the functional formulation, which is a mathematical expression for how the slant delay varies with respect to a set of parameters. The most popular closed-form expression is given by Marini (1972), which models the elevation angle component of the delay as a continued fraction form of $1/\sin(\varepsilon)$, normalized to yield unity at zenith by Herring (1992):

$$k_\varepsilon(\varepsilon) = \frac{1 + \dfrac{a}{1 + \dfrac{b}{1 + \frac{c}{\ldots}}}}{\sin(\varepsilon) + \dfrac{a}{\sin(\varepsilon) + \dfrac{b}{\sin(\varepsilon) + \frac{c}{\ldots}}}} \tag{4}$$

Marini (1972) found that by truncating the continued fraction form at four coefficients, it was possible to introduce an error of only 0.1 % of the delay at the 1° elevation angle, compared to ray-tracing of an exponential, azimuthally symmetric atmospheric profile. Due to the high accuracy of this functional formulation, it has been adopted in the realization of all state-of-the-art mapping functions currently in use today.

The realization of the Marini formulation, i.e., the particular values assigned to the *a, b, c* coefficients, differs for the commonly used mapping functions, having various sources of atmospheric data, parameterization of the coefficients and ray-tracing algorithms in the calibration of the coefficients. All of these mapping functions make a similar assumption of a spherically symmetric atmosphere, relying on only a vertical profile of the atmosphere and ignoring any variation of the delay as a function of azimuth.

Experiment description

Here, we describe the ray-tracing campaign used to evaluate the underlying functional formulations as well as review the current state-of-the-art mapping functions used for geodetic purposes.

Ray-tracing campaign

The slant delays used as truth values in the analysis are determined by ray-tracing through the Canadian Meteorological Centre's Global Environment Mesoscale (CMC-GEM) analysis. The CMC-GEM is available on a 6 h basis starting at midnight UTC. The global analysis has a grid resolution of 0.6° in latitude and 0.6° in longitude and 28 isobaric levels and additionally on a terrain-following near-surface level.

The ray-path is modeled as a bent-2D curve. Under this assumption, the contribution of the out of plane bending of the ray is neglected, which was shown in Nievinski and Santos (2010) to be negligible except under extreme conditions. The full three-dimensional atmospheric model is used, making no assumptions about its structure or the variation of the atmospheric parameters. An ellipsoidal earth model is used for the three-dimensional ray-tracing. For more details on the ray-tracing algorithms, please refer to Nievinski and Santos (2010).

Several possibilities exist for choosing the observation geometry for the assessment. Ichikawa et al. (2008) chose satellite geometry based on a realistic GPS constellation to simulate the effect on receiver position of tropospheric slant delay errors. Eresmaa et al. (2008) used a homogenous distribution of 67 hypothetical satellite positions, while Hobiger et al. (2010) and Pany et al. (2009) chose to ray-trace on a dense 1° × 1° grid of the entire sky, from 3° to 90° elevation angle, in order to obtain a nearly complete representation of the atmosphere. To achieve a substantial time series on a global set of stations, this approach was deemed impractical. Instead, we have tried to find a compromise between the methods above, as follows.

In terms of elevation angle, it is well known that the delay increases at a rate approximately equal to $1/\sin(\varepsilon)$.

Therefore, it would seem appropriate to choose to ray-trace at elevation angles that are evenly spaced in $1/\sin(\varepsilon)$. In terms of azimuth, the spacing between the ray-traced observations will be a function of the resolution of the NWM, as well as the distance between the exit points of adjacent rays in the atmosphere. Based on these criteria, a spacing of 10° in azimuth was deemed sufficient for having a realistic representation of the spatial variability of the delay, while elevation angles of 3°, 5°, 7°, 10°, 14°, 20°, 40°, 70°, and 90° were chosen, similar to those chosen by Boehm and Schuh (2004). The cutoff elevation angle of 3° was chosen as the mapping functions evaluated in this research are only valid to this elevation angle. Selective tests on two sites were carried out using this spacing and compared to a dense 1° × 1° spacing, and the discrepancies were negligible; therefore, the reduced spacing was deemed adequate.

Twenty stations from the IGS network (Dow et al. 2009) were chosen for the subsequent analysis. These stations provide a representative sample of various atmospheric conditions and include northern, equatorial, and southern hemisphere locations.

State-of-the-art mapping functions

Many mapping functions have been proposed in the past, but only a few have been widely adopted for geodetic positioning purposes on a routine basis. Niell (1996) developed both a hydrostatic and a non-hydrostatic mapping function valid down to 3° elevation angle based on the continued fraction expression of Marini (1972) truncated at the third term. The NMF was realized by a ray-tracing campaign performed through temperature and humidity profiles given at predefined pressure levels obtained from the US Standard Atmosphere. The three coefficients for both the hydrostatic and non-hydrostatic mapping function are calibrated by means of a least squares fit of nine ray-traces calculated between 3° and 90° in a spherically symmetric atmosphere.

The Vienna Mapping Function 1 (VMF1), described in Boehm et al. (2006b), is based on ray-tracing through the European Center for Medium-range Weather Forecasts (ECMWF) operational analysis at a single elevation angle of 3.3°. The *b* and *c* coefficients are computed by an empirical formulation, while the *a* coefficient is determined on a sub-daily basis via ray-tracing through a spherically symmetric atmosphere. The VMF1 was originally site specific, but a gridded version has also been introduced. We have chosen the site-VMF1 for the analysis, but as Kouba (2008) found negligible differences between the gridded and site VMF1, the results should be applicable to both.

As the VMF1 is produced using the ECMWF NWM, we also determine a separate VMF1 by ray-tracing through the

CMC-GEM under the assumption of a spherical osculating atmosphere, using the UNB ray-tracing algorithms. This is done to prevent any differences in the atmospheric source from influencing the performance of the VMF1 functional formulation with respect to the three-dimensional ray-traced truth data. The earth model used for this mapping function differs from the truth data set in that a Gaussian earth radius is assumed rather than an ellipsoidal model. We refer to this mapping function as the UNB-VMF1.

The GMF (Boehm et al. 2006a) was developed as a lower-resolution, closed-form version of the VMF1 mapping functions. The advantage of the GMF is that no external input files are required. Like the VMF1, the GMF uses the Marini functional formulation. The b and c coefficients for both the hydrostatic and non-hydrostatic mapping functions are obtained from the VMF1. The a coefficient is determined by ray-tracing through monthly mean values of pressure, temperature, and humidity obtained from the ECMWF 40-year re-analysis data, which was produced on a $15° \times 15°$ grid for the a period from September 1999 to August 2002. The same data set was utilized to develop in parallel the Global Pressure and Temperature (GPT) model (Boehm et al. 2007), aimed at the determination of a priori hydrostatic zenith delays.

An improved version of the combined GMF and GPT models, called simply GPT2, was developed by Lagler et al. (2013). It is based on 10 years of ECMWF data and is provided on a global $5° \times 5°$ grid. These values are provided at mean ETOPO5-based heights. The GPT2 includes both annual and semi-annual variations.

Results and discussion

We begin the assessment by evaluating the underlying functional formulations used in the state-of-the-art mapping functions. We then compare how the realizations of those coefficients, as realized by the various state-of-the-art mapping functions, perform compared to the three-dimensional ray-tracing.
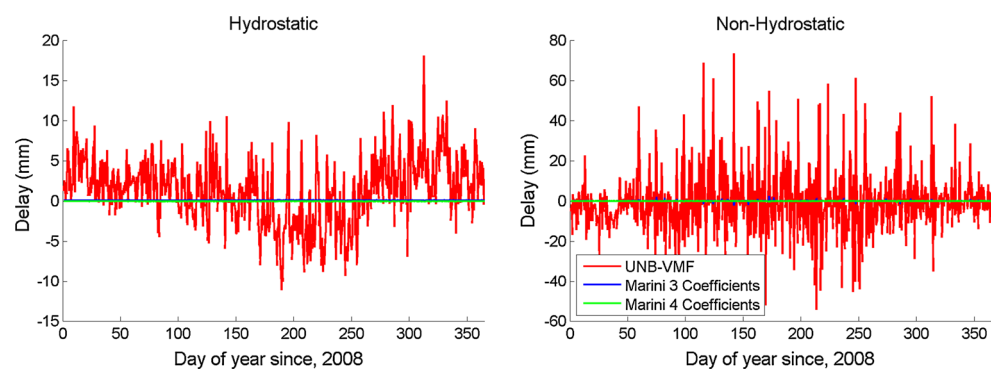
Assessment of functional formulations

The purpose of the functional formulation assessment is to identify how the choice of coefficients values in the Marini expression affects the overall accuracy of the slant factor model. For the Marini expression, we evaluate the effect of truncating the continued fraction form at its traditional three coefficients as well as including a fourth coefficient, referred to as Marini 3 and Marini 4, respectively. We have also included the VMF1 parameterization which uses empirical expressions for the b and c coefficients of the Marini expression to evaluate the effect of these assumptions on the end performance. For the Marini 3 and Marini 4, all coefficients are estimated, while for the VMF1 parameterization, only the a coefficient is estimated. The fitting of the Marini functional formulations was achieved using a nonlinear least squares approach; partial derivatives were obtained numerically.

Figure 1 shows the twice daily mean bias at the 5° elevation angle for the hydrostatic and non-hydrostatic functional formulations for a single station, YSSK. The bias in the slant factor has been multiplied by a nominal zenith hydrostatic of 2,300 mm and non-hydrostatic zenith delay 220 mm to convert the unitless slant factor bias to units of length. It is possible to see that the use of the empirical coefficients for the VMF1 functional formulation introduces some seasonal error in the slant factor. This implies that the a coefficient alone cannot model all of the variability of the slant factor on a day-to-day basis. When all coefficients of the Marini expressions are fit, the day-to-day variability is nearly completely modeled for both hydrostatic non-hydrostatic components.

Figures 2 and 3 show the mean and standard deviation of the biases for the different functional formulations, including the VMF1 parameterization over all stations for the year 2008. For the hydrostatic component (Fig. 2) and the non-hydrostatic component (Fig. 3), both Marini 3 and Marini 4 perform very well. The addition of the fourth coefficient tends to result in slightly smaller biases than the three coefficient formulation, although for both cases the

Fig. 1 Twice daily mean biases of the hydrostatic (*left*) and non-hydrostatic (*right*) functional formulations for the year 2008 with respect to the three-dimensional ray-tracing at 5° elevation angle for station Yuzhno-Sakhalinsk, Russia (YSSK). Please note the difference in *vertical* scales
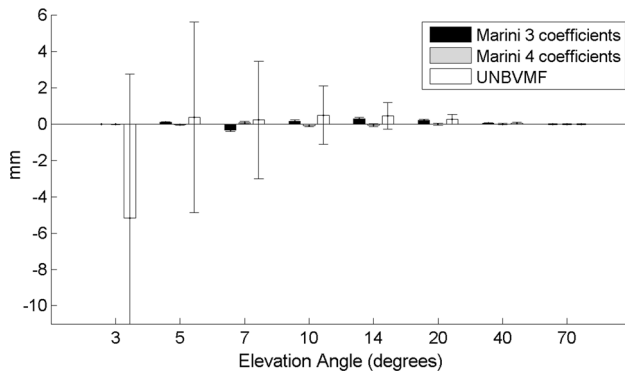
Fig. 2 Mean bias of the slant factors for the hydrostatic functional formulations for each elevation angle used in the assessment. The *error bar* indicates the standard deviation of the daily biases over all stations and all epochs in the year 2008
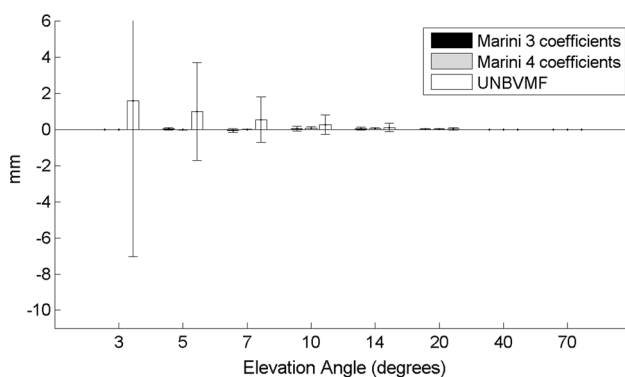

Fig. 3 Mean bias of the slant factors for the non-hydrostatic functional formulation for each elevation angle used in the assessment. The *error bar* indicates the standard deviation of the daily biases over all stations and all epochs in the year 2008

biases remain under 0.5 mm for all elevation angles assessed. For the VMF1 realization, above 5° elevation angle, the bias is less than 1 mm, but at the 3° elevation angle the bias approaches 5 mm in slant delay, with a slightly larger standard deviation.

The main advantage of either Marini 3 or 4 is the improvement in the standard deviation when compared to the empirical coefficients used for the VMF1 formulation. When all three coefficients are estimated, all of the day-to-day variability is modeled. The approach of estimating all three of the Marini coefficients was discussed in Boehm and Schuh (2004), referred to as the rigorous VMF1. However, to our knowledge, no comparisons in the position domain have been performed as the rigorous approach requires more numerous ray-tracings.

Assessment of mapping functions

We now assess the performance of the state-of-the-art mapping function calibrations described in Section "State-of-the-art mapping functions," namely the NMF, GMF, GPT2, and VMF1. For the VMF1 and GPT2, both sub-daily calibrations are used as input for the *a* coefficients. The error in the mapping functions has been multiplied by the mean zenith delays for each site to obtain an equivalent error in slant delay. In order to quantify the effect of this error on station height estimates, we have used the rule-of-thumb proposed by MacMillan and Ma (1998), also adopted by Boehm (2008), namely that the error in station height is equal to 1/5 the error in the slant delay at the lowest elevation angle included in the analysis. For this research, a cutoff elevation angle of 5° is adopted, as in Boehm et al. (2008).

Figure 4 shows the mean difference in station height for the hydrostatic mapping functions with respect to the three-dimensional ray-tracing. For the NMF, the largest errors occur in the southern latitudes, most notably OHI2, which has a bias of nearly 9 mm. This is in agreement of other studies, which have found a systematic bias in the station heights for the NMF for stations located in this region when compared to NWM-based mapping functions (Boehm et al. 2006b; Vey et al. 2006). GPT2 performs very well for a climatological mapping function. A small improvement is seen when compared to the GMF, which has an overall RMS of 1.4 mm as compared to 1.0 mm for GPT2. Therefore, it is further evidence for the recommendation of the GPT2 as an acceptable backup when the VMF1 is not available.

Good agreement was found between UNB-VMF1 and VMF1. The former agrees better with the three-dimensional ray-tracing, having smaller overall RMS and standard deviations for the individual stations. This is expected as they share the same atmospheric data source.

Figure 5 presents several examples of the daily biases at the 5° elevation angle for the NMF, GMF, GPT2, VMF1, and UNB-VMF1 hydrostatic mapping functions over the year 2008. In this case, the slant factors were multiplied by a nominal zenith hydrostatic delay of 2,300 mm to remove any sub-annual variability caused by changes in the actual average zenith hydrostatic delay.

Several sub-annual signals can be seen as a result of the different mapping function, particularly for the NMF at stations NICO and POL2. These signals also appear in the GMF results albeit the magnitude tends to be smaller, being further reduced with the GPT2. Both the VMF1 and UNB-VMF1 provide excellent agreement with respect to the three-dimensional ray-tracing and are able to model the daily variation in the slant factor. This demonstrates the importance of using NWM-derived mapping functions when attempting to identify seasonal or sub-annual trends in station time series. Additionally, the good agreement between the VMF1 and UNB-VMF1 indicates that the two NWM,

Fig. 4 Mean difference in
station height (following 1/5
rule-of-thumb) in millimeters
for the hydrostatic mapping
function with respect to the
three-dimensional ray-tracing.
a NMF, **b** GMF, **c** GPT2
d VMF1, **e** UNB-VMF1. Slant
factors have been multiplied by
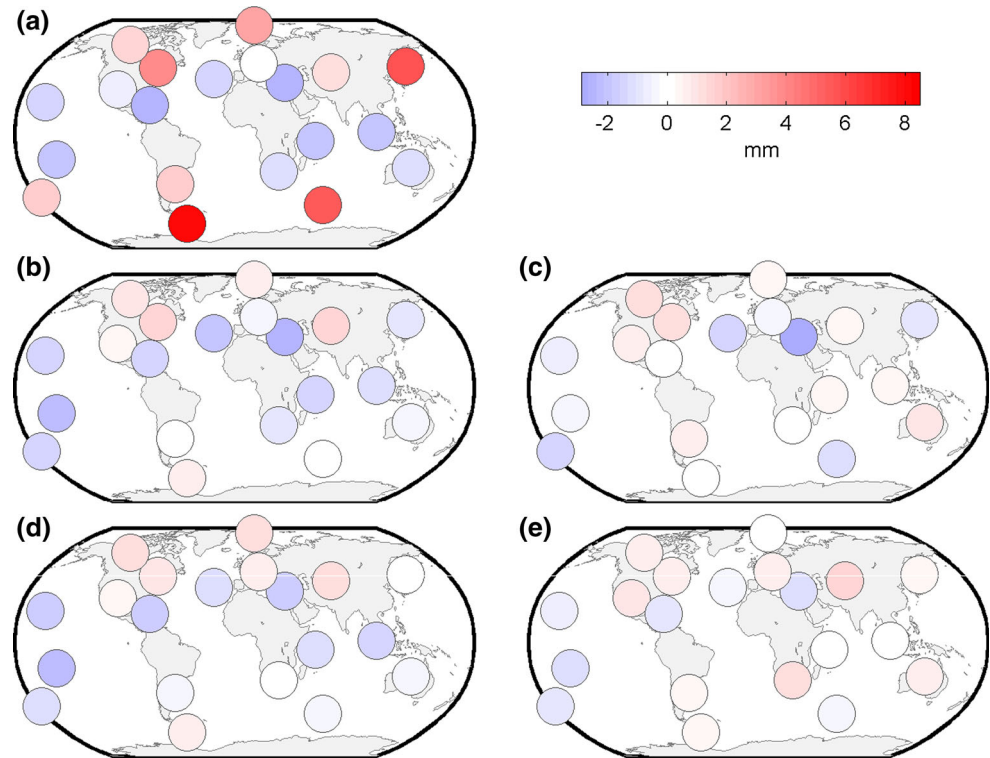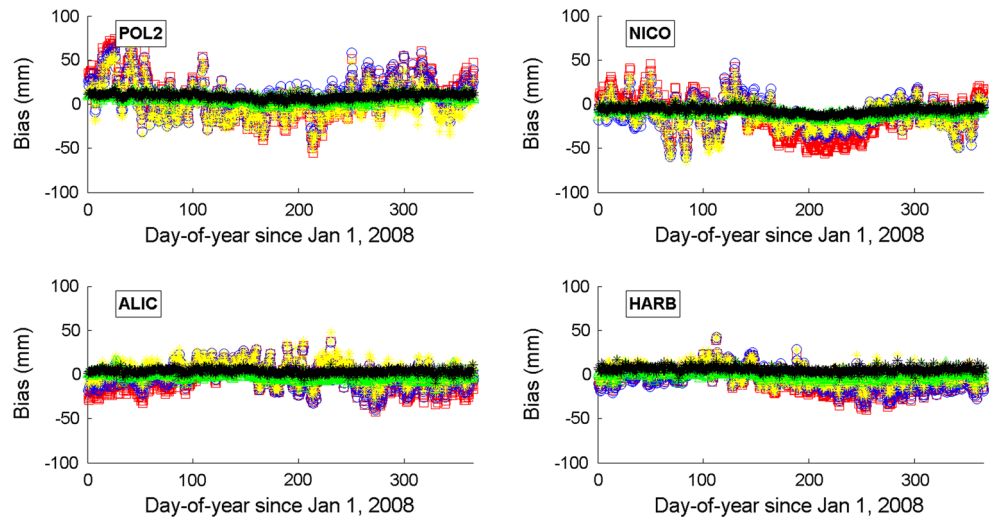the average zenith hydrostatic
delay for each site

Fig. 5 Twice daily biases in
slant delay for the hydrostatic
mapping functions at 5°
elevation angle for the year
2008, stations HARB, MDO1,
NICO, and OHI2. VMF1
(*green*), UNB-VMF1 (*black*),
GPT2 (*yellow*), GMF (*blue*),
and NMF (*red*). Slant factors
were multiplied by a nominal
zenith hydrostatic delay of
2,300 mm

ECMWF and CMC-GEM, tend to agree well for the
hydrostatic slant factor.

The main difference between the climatological and
NWM-derived mapping functions is in their daily repeatability, which is typically three to four times as large as the
NWM-based mapping functions at the 5° elevation angle.
This is due to the climatology models not capturing the
day-to-day variations of the slant factors. At higher elevation angles, these differences are smaller although may
be equally important due to elevation angle dependent
weighting employed in geodetic processing.

In Fig. 4, a small latitude-dependent bias in equivalent
station height is seen between the three-dimensional ray-tracing and the state-of-the-art mapping functions. We
attribute this bias to the simplification in the shape of the
earth used for the state-of-the-art mapping functions to a
sphere of constant radius. The UNB-VMF1 implementation adopts a Gaussian radius, $R_e = \sqrt{M \cdot N}$, where M and
N are the radii of curvature of the meridian section and of
the prime vertical section, respectively. The Gaussian
radius is a better approximation of the ellipsoidal shape of
the earth. In the case of the truth data set, an ellipsoidal

Fig. 6 Difference in mean station height between the VMF1 (*blue crosses*, *blue line*), UNB-VMF1 with Gaussian curvature radius (*black circles*, *black line*), and UNB-VMF1 with constant radius (*red squares*, *red line*). The solid lines represent a least squares fit to the mean station height biases for each time series. See Table 1 for more details
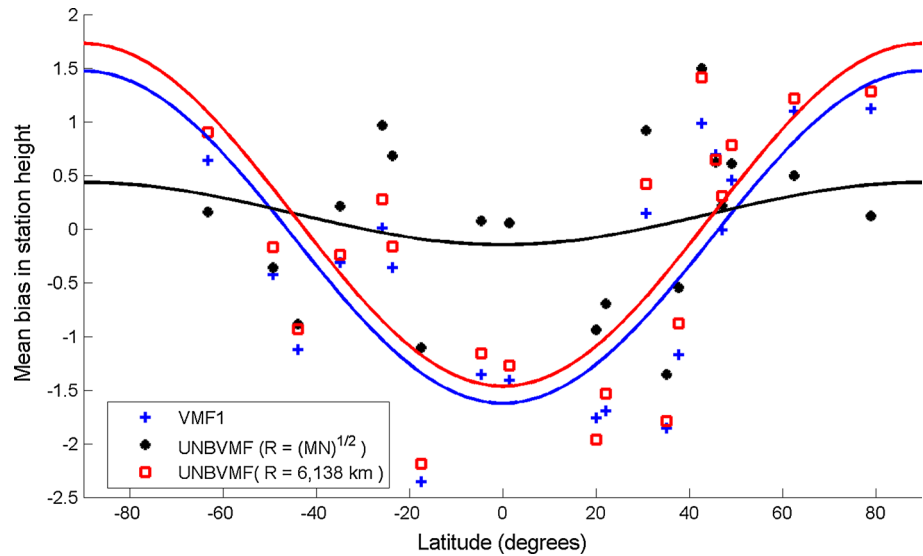
earth model is used, which is a more realistic representation considering the earth's oblateness.

Figure 6 shows the influence of radius of the earth for the VMF1 and UNB-VMF1 hydrostatic mapping functions with respect to latitude, where the error in slant delay has been converted to error in station height using the 1/5 rule-of-thumb. In order to better demonstrate how systematic this effect is, we have included a UNB-VMF1 that adopts a constant radius (red line), as used for the VMF1. The solid lines in Fig. 6 are the result of a least squares fit of the bias in station height to a sinusoid of the form $\alpha \cdot \cos(2\phi) + \beta$. The coefficients of the sinusoidal fit to the latitude-dependent biases for the VMF1 and the UNB-VMF1 with constant radius are shown in Table 1. Both the VMF1 and the UNB-VMF1 using a constant radius exhibit a similar trend while the UNB-VMF1 using the Gaussian curvature (black line) reduces this systematic trend to a negligible amount when compared to the ellipsoidal earth used in the three-dimensional ray-tracing. Overall, the use of a constant radius can introduce approximately a ±2 mm bias in station height, which is largest at the poles and at the equator. As the magnitude of the non-hydrostatic delay is an order of magnitude smaller, the effect of the earth's radius although systematic is not significant.

Figure 7 shows the bias, i.e., mean difference, in station height for the non-hydrostatic mapping functions with respect to the three-dimensional ray-tracing. As was the case for the hydrostatic mapping functions, the difference in the slant factor has been multiplied by an average non-hydrostatic zenith delay computed for each station then converted to changes in station height following the same 1/5 rule-of-thumb.

Overall, the GMF, GPT2, VMF1, and UNB-VMF1 mapping functions exhibit excellent agreement with the three-dimensional ray-tracing for the non-hydrostatic component. For GMF and GPT2, the biases typically are under 1 mm, while VMF1 and UNB-VMF1 agree to the sub-millimeter level. NMF performed slightly worse with station NICO having a bias of −5.7 mm.

Figure 8 shows the daily biases at the 5° elevation angle for the non-hydrostatic mapping functions over the year 2008 for several stations. The non-hydrostatic delay is very difficult to predict well as it is dependent on small fluctuations of water vapor in the atmosphere. For this reason even when using ray-tracing to determine the a coefficient of the Marini expression, as is the case for the VMF1 and UNB-VMF1 mapping functions, there is little improvement in the overall performance compared to the climatological mapping functions.

Some seasonal variations are present, which are related to the variability of the water vapor content present in the atmosphere. For example, southern latitude stations such as HARB tend to have better agreement between day of year 150–250 particularly for the NWM-derived mapping functions while northern hemisphere stations, such as MDO1, have better agreement between day of year 0–100.

Although the performance of the non-hydrostatic mapping functions is somewhat poor, the use of three-dimensional ray-tracing at the observation level may not help

Table 1 Coefficients of the least square fit to the mean bias in station height for VMF1, UNB-VMF1 with constant radius, and UNB-VMF1 with Gaussian radius with respect to three-dimensional ray-tracing

Mapping function	Coefficients	
	a	b
VMF1	−1.548	−0.075
UNB-VMF1 ($R = \sqrt{MN}$)	−0.290	+0.143
UNB-VMF1 ($R = 6{,}138$ km)	−1.597	+0.132

Fig. 7 Difference in station height in millimeters (following 1/5 rule-of-thumb) for the non-hydrostatic mapping function with respect to the three-dimensional ray-tracing. **a** NMF, **b** GMF, **c** GPT2 **d** VMF1, **e** UNB-VMF1. Slant factors have been multiplied by the average zenith non-hydrostatic delay for each site. The color bar has been clipped at ±4 mm for greater discrimination of non-NMF results
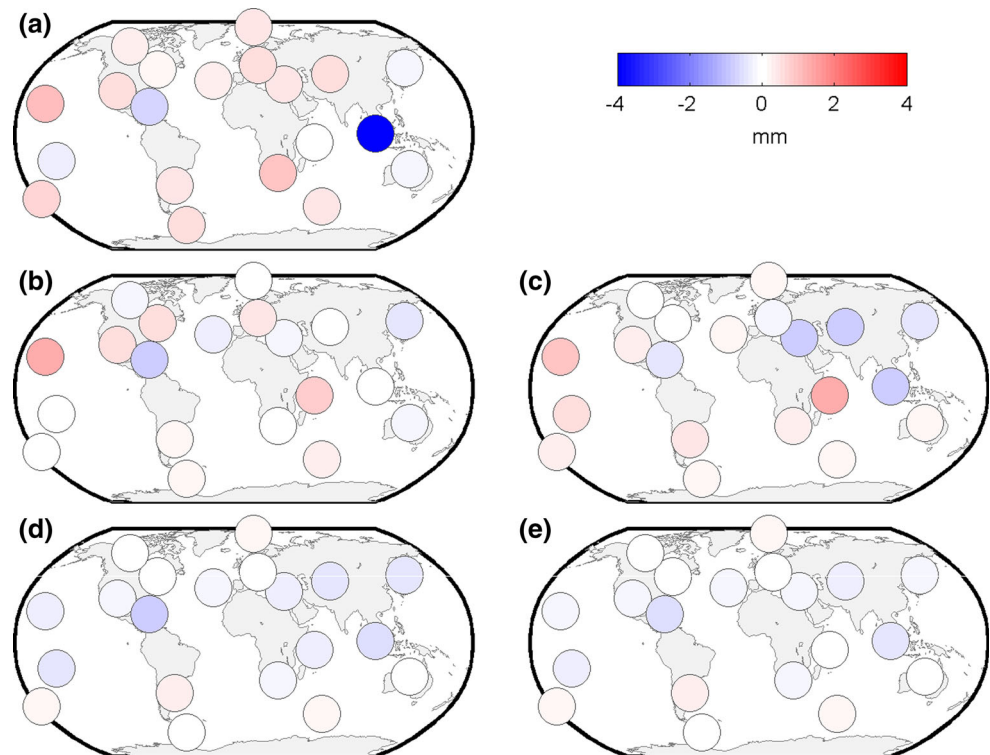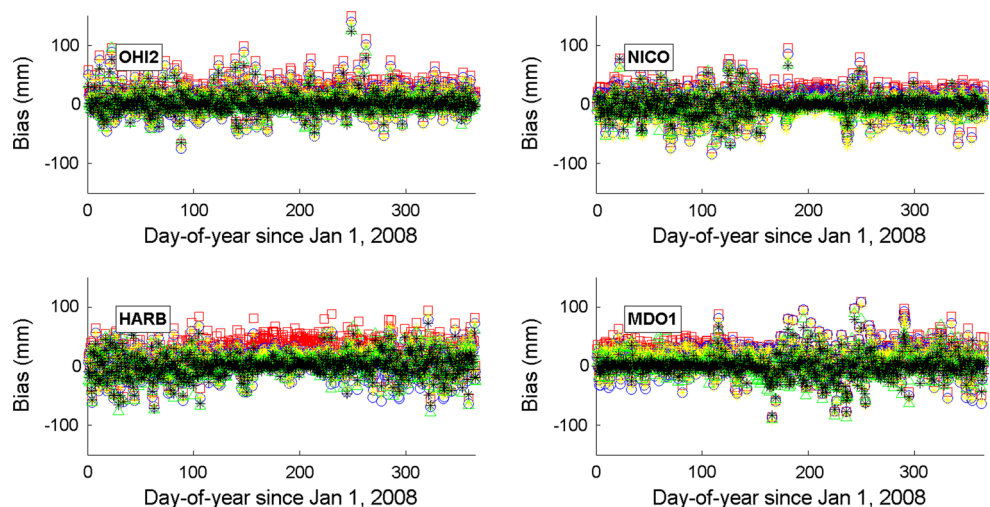

Fig. 8 Twice daily biases in slant delay for the non-hydrostatic mapping functions at 5° elevation angle of for the year 2008, stations HARB, MDO1, NICO, and OHI2. VMF1 (*green*), UNB-VMF1 (*black*), GPT2 (*yellow*), GMF (*blue*) and NMF (*red*). Slant factors were multiplied by a nominal zenith non-hydrostatic delay of 220 mm

alleviate this problem; the small-scale water vapor fluctuations are unlikely to be resolved even by fine-mesh NWM as the underlying physical processes are difficult to capture.

Conclusions

The current state-of-the-art mapping functions and functional formulations used for space geodetic techniques have been assessed. This was the first global evaluation of these mapping functions using three-dimensional ray-tracing. Additionally, the fitting of the Marini functional formulation to three-dimensional ray-traced slant factors was investigated to identify any deficiencies in the $1/\sin(\varepsilon)$ expansion.

The Marini functional formulation truncated at three coefficients was found to be adequate for modeling the elevation angle dependence of the three-dimensional tropospheric slant factors to an accuracy better than 1 mm down to the 3° elevation angle. A slight improvement was found when a fourth coefficient was included although the improvement was not found to be a large enough to warrant the adoption of this model. The use of the VMF1 parameterization could be improved by estimating all three of the

Marini coefficients rather than using the empirical b and c coefficients, although an improvement in the position domain would need to be demonstrated.

In terms of the mapping functions, the VMF1 performed remarkably well, introducing less than 1 mm bias in equivalent station height with respect to the three-dimensional ray-tracing. This finding lends weight to the recommendation of VMF1 as the most accurate mapping function for geodetic applications. The importance of using NWM-based mapping functions when investigating inter-annual geophysical signals was identified as the climatological mapping functions (GMF, GPT2) are unable to model the seasonal variability of the slant factors.

A small latitude-dependent error was found in the hydrostatic mapping functions, which was attributed to the assumption of a constant radius spherical earth. This was reduced when a Gaussian curvature radius was used. Also, the GPT2 was found to be a good back up for NWM-based mapping functions as it did not introduce a significant bias with respect to the VMF1, although a worse repeatability is to be expected. This is in agreement with the current IERS recommendations.

A new realization of the VMF1 has also been introduced, which is referred to as the UNB-VMF1. Using the Canadian NWM (CMC-GEM) as its atmospheric source, it was demonstrated to agree well with VMF1, which relies on the ECMWF analysis. These results have led to the development of a service, which produces similar sub-daily products using both the CMC-GEM and NCEP re-analysis, available at http://unb-vmf1.gge.unb.ca/.

References

Boehm J, Schuh H (2004) Vienna mapping functions in VLBI analyses. Geophys Res Lett 31:L01603. doi:10.1029/2003GLO18984

Boehm J, Niell AE, Tregoning P, Schuh H (2006a) Global Mapping Function (GMF): A new empirical mapping function based on numerical weather model data. Geophys Res Lett 33:L07304-1–L07304-4. doi:10.1029/2005GL025546

Boehm J, Werl B, Schuh H (2006b) Troposphere mapping functions for GPS and very long baseline interferometry from European Centre for Medium-Range Weather Forecasts operational analysis data. J Geophys Res 111:B02406. doi:10.1029/2005JB003629

Boehm J, Heinkelmann R, Schuh H (2007) Short note: a global model of pressure and temperature for geodetic applications. J Geod 81(10):679–683. doi:10.1007/s00190-007-0135-3

Boehm J, Kouba J, Schuh H (2008) Forecast vienna mapping functions 1 for real-time analysis of space geodetic observations. J Geod 83:397–401. doi:10.1007/s00190-008-0216-y

Dow JM, Neilan RE, Rizos C (2009) The international GNSS Service in a changing landscape of global navigation satellite systems. J Geod 83:191–198. doi:10.1007/s00190-008-0300-3

Eresmaa R, Nordman M, Poutanen M, Syrjärinne J, Luntama J-P, Järvinen H (2008) Parameterization of tropospheric delay correction for mobile GNSS positioning: a case study of a cold front passage. Meteorol Appl 15:447–454. doi:10.1002/met.86

Herring TA (1992) Modelling atmospheric delays in the analysis of space geodetic data. In: de Munck JC, Spoelstra TAT (eds) Proceedings of the symposium refraction of transatmospheric signals in geodesy. The Netherlands, The Hague, pp 157–164

Hobiger T, Shimada S, Shimizu S, Ichikawa R, Koyama Y, Kondo T (2010) Improving GPS positioning estimates during extreme weather situations by the help of fine-mesh numerical weather models. J Atmos Sol-Terr Phys 72:262–270. doi:10.1016/j.jastp.2009.11.018

Ichikawa R, Hobiger T, Koyama Y, Kondo T (2008) An evaluation of the practicability of current mapping functions using ray-traced delays from JMA mesoscale numerical weather data. Proceedings of the international symposium on GPS/GNSS. The Institute of Positioning, Navigation and Timing of Japan, Tokyo, Japan, pp 5–12

Kouba J (2008) Implementation and testing of the gridded Vienna Mapping Function 1 (VMF1). J Geod 82:193–205. doi:10.1007/s00190-007-0170-0

Lagler K, Schindelegger M, Böhm J, Krásná H, and Nilsson T (2013) GPT2: empirical slant delay model for radio space geodetic techniques. Geophys Res Lett 40:1069–1073. doi:10.1002/grl.50288

MacMillan DS, Ma C (1998) Using meteorological data assimilation models in computing tropospheric delays at micrwave [sic] frequencies. Phys Chem Earth 23:97–102. doi:10.1016/S0079-1946(97)00249-8

Marini JW (1972) Correction of satellite tracking data for an arbitrary tropospheric profile. Radio Sci 7:223–231. doi:10.1029/RS007i002p00223

Niell AE (1996) Global mapping functions for the atmosphere delay at radio wavelengths. J Geophys Res 101:3227–3246. doi:10.1029/95JB03048

Nievinski FG, Santos M (2010) Ray-tracing options to mitigate the neutral atmosphere delay in GPS. Geomatica 64:191–207

Pany A, Boehm J, Schuh H, Hobiger T, Ichikaya R (2009) Modeling azimuthal asymmetries of the troposphere delay during a 14-days typhoon period in Tsukuba. Proceedings of the 19th Working Meeting on European VLBI for Geodesy and Astrometry

Rüeger JM (2002) Refractive index formulae for radio waves. FIG XXII International Congress, Washington, DC., USA, April 19-26

Tesmer V, Boehm J, Heinkelman R, Schuh H (2007) Effect of different tropospheric mapping functions on the TRF, CRF and position time-series estimated from VLBI. J Geod 81:409–421. doi:10.1007/s00190-006-0126-9

Urquhart L, Nievinski FG, Santos MC (2012) Ray-traced slant factors for mitigating the tropospheric delay at the observation level. J Geod 86:149–160. doi:10.1007/s00190-011-0503-x

Vey S, Dietrich R, Fritsche M, Rülke A, Rothacher M, Steigenberger P (2006) Influence of mapping function parameters on global GPS network analyses: comparisons between NMF and IMF. Geophys Res Lett 33:L01814. doi:10.1029/2005GL024361

Author Biographies

Landon Urquhart is a GNSS Research Engineer at Nexteq Navigation in Calgary, Canada. He obtained his B.Sc. and M.Sc. in Geodesy and Geomatics Engineering at the University of New Brunswick. His research interests include using numerical weather models for geodetic positioning and precise point positioning with ambiguity resolution. He is an Alberta Innovates R & D Associate.

Marcelo Santos is a Professor in the Department of Geodesy and Geomatics Engineering at the University of New Brunswick, Canada. He holds a M.Sc. Degree in Geophysics from the National Observatory, in Rio de Janeiro, and a Ph.D. Degree in Geodesy from the University of New Brunswick. He is president of the International Association of Geodesy Sub-Commission 4.3 on remote sensing and modeling of the atmosphere. His research relates to Gravity Field and Global Navigation Satellite Systems.

Felipe G. Nievinski is a post-doctoral researcher at UNESP, Brazil, where he works in the field of GPS multipath reflectometry. He earned his PhD (Aerospace) from the University of Colorado Boulder in 2013, M.Sc.E. (Geodesy) from the University of New Brunswick in 2009, and B.E. (Geomatics) from UFRGS, Brazil, in 2005.